scientific reports

Check for updates

OPEN

Development of an acute lung injury model for drug testing

Jocelyn R. Grunwell[1,2]✉, Susan T. Stephenson[2], Gail A. Dallalio[2], Badiallo A. Diani[3], Celena Zaworski[1], Natalie Jordan[1] & Anne M. Fitzpatrick[2]

A challenge that limits our understanding of the underlying pathobiology of pediatric acute respiratory distress syndrome (PARDS) is the lack of a preclinical airway model that can be leveraged for the study of mechanisms and specific molecules for drug testing. We developed a physiologic model system of the small airways for mechanistic application in PARDS using a co-culture of primary human-derived small airway epithelial cells (SAECs) cultured at the air–liquid interface and umbilical vein endothelial cells in a transwell system. The model was validated by exposing the SAECs to a rhinovirus infection, to an inflammatory lung insult using a mixture of cytokines found in ARDS (cytomix), and to airway fluid samples from children with different severity strata of PARDS. We used a combination of transepithelial electrical resistance, immunofluorescence confocal microscopy of tight junctions, targeted gene expression, and cytokine responses to evaluate the model to the aforementioned insults. We then use the model in drug testing and show the reduction in IL-6 expression in conditioned media and STAT3 phosphorylation following co-treatment of SAECs with cytomix and the Janus kinase inhibitor (JAKi) baricitinib. This model enables mechanistic studies of airway pathobiology and may serve as a novel drug testing platform for PARDS.

Keywords Pediatric, Acute respiratory distress syndrome, Baricitinib, STAT3, Small airway epithelial cells, Model

Pediatric acute respiratory distress syndrome (**PARDS**) is the most severe form of acute lung injury that occurs in 6.1% of mechanically ventilated children in the Pediatric Intensive Care Unit (**PICU**)[1]. PARDS is an immune-mediated syndrome that frequently results from respiratory infections and is accompanied by infiltrates on a chest radiograph and sustained hypoxemia due to noncardiogenic pulmonary edema that is not solely attributed to fluid overload[2–4]. Children with severe hypoxemia account for ~ 30% of PARDS cases, and ~ 30% of these children die[1]. However, despite the morbidity and mortality of PARDS, only supportive therapies, such as lung-protective mechanical ventilation, are available. Consequently, the pathobiology of PARDS remains somewhat unclear and there is little available evidence to direct pharmacotherapy, creating a significant knowledge gap.

A major challenge associated with knowledge generation in PARDS is the lack of a preclinical model that can be leveraged for the study of specific molecules[2,5]. While substantial research has characterized the plasma biomarkers associated with PARDS severity and outcomes[6–11], there is far less investigation into the underlying mechanisms of airway immune dysregulation in PARDS. This is in part due to the invasive nature of biological airway sampling and ethical challenges associated with research in critically ill children. However, the air space is where the most substantial injury occurs, and new biological insight is essential for development of new pharmacotherapies for PARDS.

To address this gap, we developed a physiologic model system of the small airways for mechanistic application in PARDS. This model system contains primary small airway epithelial cells (SAECs) and human umbilical vein vascular endothelial cells (HUVECs), since both epithelial and endothelial injury are hallmarks of PARDS. After demonstration of physiologic relevance, the model was validated by exposing the SAECs to a rhinovirus infection, to an inflammatory lung insult using a mixture of cytokines found in ARDS (cytomix), and with airway fluid samples from children with different severity strata of PARDS. The Janus kinase/signal transducer and activator of transcription (JAK/STAT) pathway, principally interleukin-6 (IL-6) mediated activation of STAT3, has emerged as a potential therapeutic target for treating adults with ARDS with recent clinical trials of the JAK inhibitor, baricitinib, demonstrating efficacy for COVID-19-triggered ARDS[12–14]. Therefore, the utility of the model for drug candidate testing was also demonstrated by using baricitinib to inhibit the JAK/STAT/IL-6 pathway to halt the inflammatory response that can lead to ARDS/PARDS.

[1]Division of Critical Care Medicine, Children's Healthcare of Atlanta, Arthur M. Blank Hospital, 2220 North Druid Hills Rd NE, Atlanta, GA 30329, USA. [2]Department of Pediatrics, Emory University School of Medicine, Atlanta, GA, USA. [3]Department of Biomedical Engineering, Georgia Institute of Technology, Atlanta, GA, USA. ✉email: jocelyn.grunwell@emory.edu

Results

Development and evaluation of the airway model

The airway model was established with SAECs and HUVECs on opposing sides of a transwell membrane, as shown in Fig. 1. Experiments were performed between days 28–35 after measuring the trans-epithelial electrical resistance (TEER) measurement to quantify barrier integrity and microscopic visualization of tight junctions[15]. We first demonstrated cellular structural integrity with confocal microscopy of the apical (epithelial) and basal (endothelial) membrane, which revealed intact cellular morphology (Fig. 2A–C) and epithelial tight junctions (Fig. 2D). We then evaluated TEER, which was slightly higher in the model than in SAECs alone (Fig. 2E). Secretion of the epidermal growth factor (EGF) and vascular endothelial growth factor A (VEGF-A) were higher on the basal side of the model compared to the apical side of the model or to SAECs alone, highlighting the compartmental effects of the model (Fig. 2F–G).

Since many cases of PARDS result from direct lung injury (i.e., pneumonia) attributed to viral lower respiratory tract infections[1,12,16,17], we next examined the performance of the model after exposure to human rhinovirus. Rhinovirus is a prevalent respiratory virus associated with lower respiratory infection in young children and frequently found in intubated children with PARDS[16,18]. For these experiments, we used the experimental RV16 strain, a major group rhinovirus which preferentially binds to intercellular adhesion molecule-1 (ICAM-1) on the surface of ciliated epithelial cells, initiating an anti-inflammatory and anti-viral interferon response[19]. Consistent with other reports[20–22], RV16 infection increased epithelial CXCL10 (also known as interferon-γ inducible protein 10 kDa [IP-10]), soluble ICAM-1, and interleukin-6 (IL-6) protein secretion (Fig. 3A–C). RV16 infection also decreased TEER (Fig. 3D) and locally altered the distribution of the tight junction proteins epithelial zona occludens protein-1 (ZO-1) and E-cadherin (Fig. 3E). RV16 treatment and RV16 followed by lipopolysaccharide (RV16 + LPS) treatment—used to mimic a secondary bacterial pneumonia following a

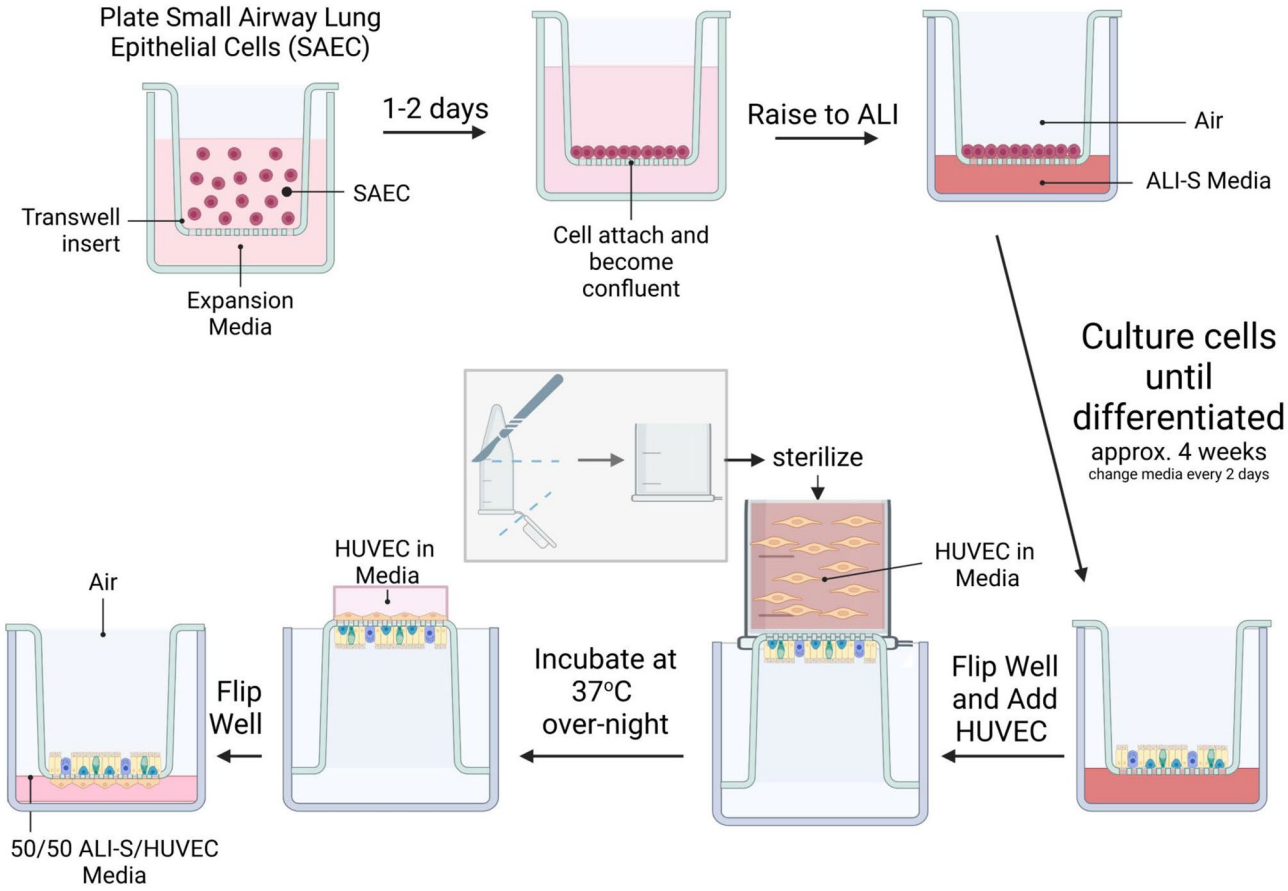

Fig. 1. Schematic of the making of the small airway epithelial cell (SAEC) and human umbilical vein endothelial cell (HUVEC) model. SAEC cells are plated in a transwell insert with expansion media for 3–4 days. Once SAEC attach to the insert and become confluent, the media from the upper chamber is removed and the SAECs are exposed to air on the apical side and air–liquid interface (ALI)-S media on the basal side of the transwell. Media is changed every 2 days during the differentiation process. After approximately 4 weeks the SAECs at ALI differentiate into mature SAECs comprised of basal, club, goblet, and ciliated cells. The transwell insert is inverted and HUVECs are added and allowed to adhere overnight at 37 °C to the underside of the transwell insert using a sterile Eppendorf tube as a protective vessel for media and cells. Once the HUVECs attach, the transwell insert is flipped over and the HUVECs are exposed to 50/50 (volume %) ALI-S/HUVECs media while the SAECs are exposed to air. Created with BioRender.com.

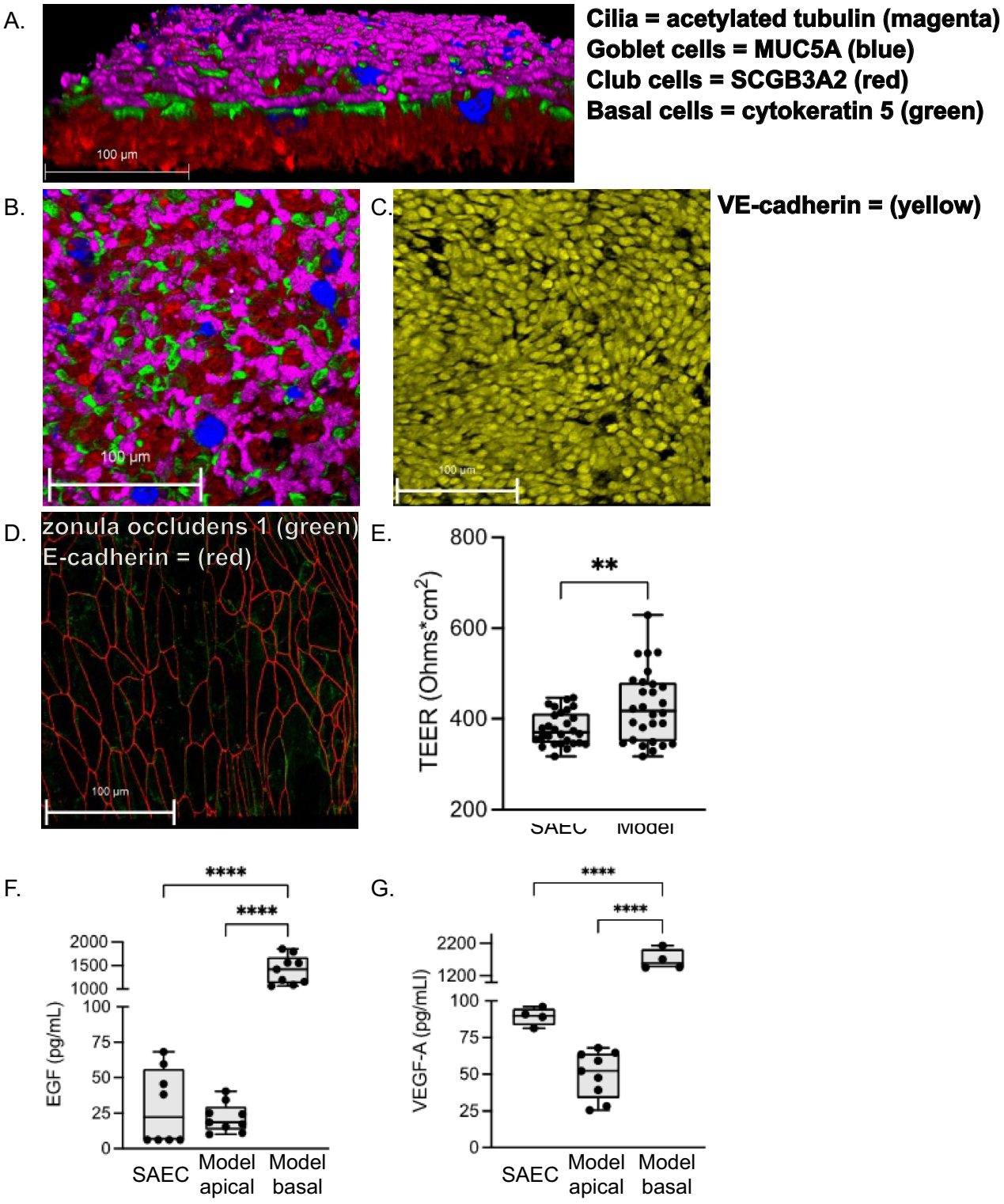

Fig. 2. Airway model with small airway epithelial cells (SAECs) on the apical side and human umbilical vein endothelial cells (HUVECs) on the basal side. (**A**) Confocal immunofluorescence microscopy images, visualized using LASX 3D Viewer, of the co-culture showing the differentiated SAEC cell types including cilia (acetylated tubulin-AF647, magenta), goblet cells (MUC5AC-AF405, blue), club cells (SCGB3A2-AF555, red), and basal cells (cytokeratin 5-AF488, green). Panel (**B**) depicts the apical SAEC layer and panel (**C**) the basal HUVECs (VE-cadherin-AF594 (yellow) layer of the model. Panel (**D**) (apical) depicts tight junctions (zonula occludens-1-AF647, green; E-cadherin-AF488, red; overlay in yellow). Panel (**E**) depicts the epithelial trans-epithelial electrical resistance (TEER). Panels (**F**) and (**G**) depict epidermal growth factor (EGF) and vascular endothelial growth factor (VEGF-A) protein secretion for 2 independent experiments with 4 replicates per experiment. $^{*}p < 0.05$, $^{**}p < 0.01$, $^{***}p < 0.001$, $^{****}p < 0.0001$.

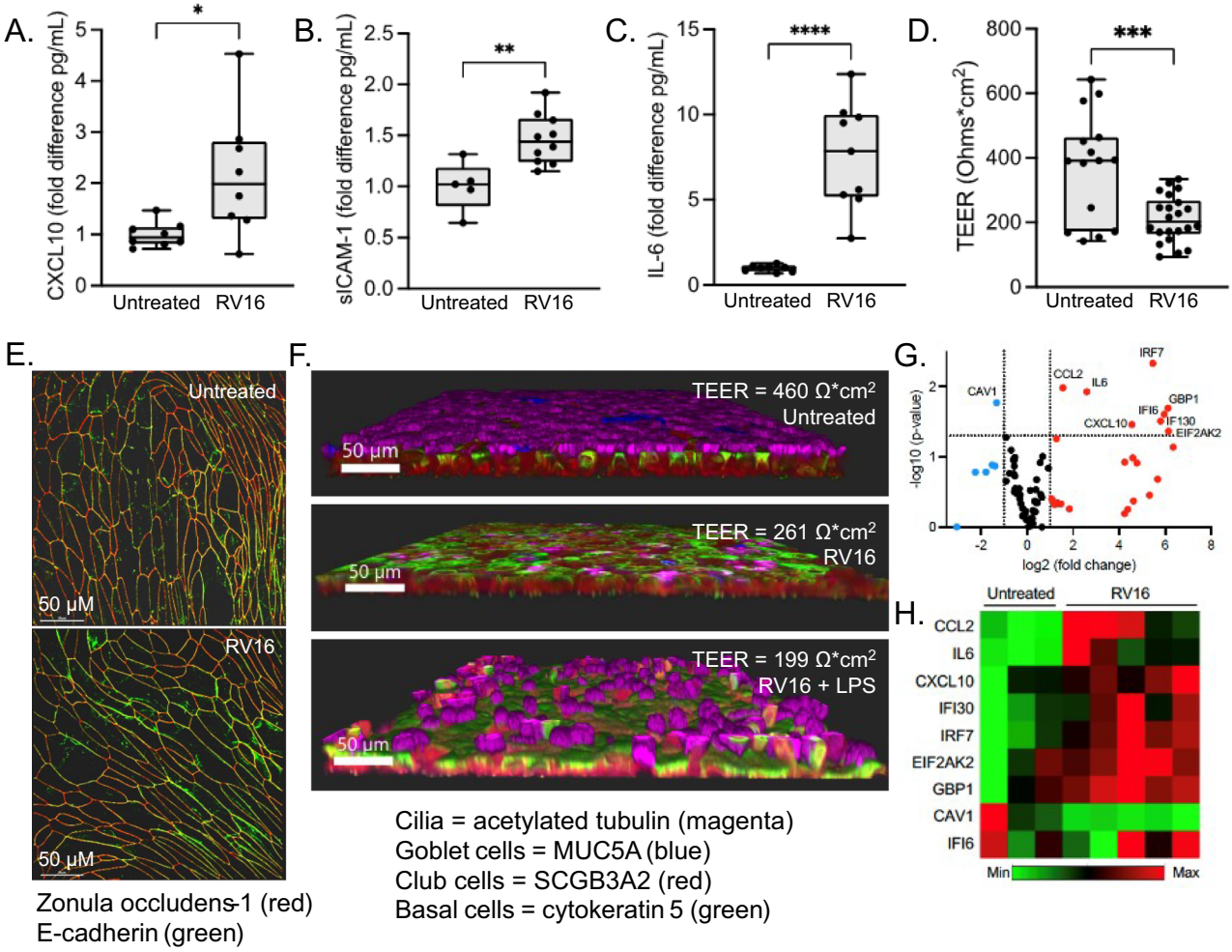

Fig. 3. Exposure of the small airway epithelial cells (SAECs) in the model to experimental rhinovirus 16 (RV16). Fold change in cytokine expression of SAECs following RV16 treatment compared to untreated control for (**A**) C-X-C motif chemokine ligand 10 (CXCL10), (**B**) soluble intercellular adhesion molecule-1 (sICAM-1), and (**C**) interleukin-6 (IL-6). (**D**) Transepithelial electrical resistance (Ω^*cm^2) in untreated (control) and RV16 treated SAECs for 2 independent experiments with 4 replicates per experiment. (**E**) Confocal immunofluorescence microscopy images, visualized using LASX 3D Viewer, of tight junctions (zonula occludens-1-AF647, red; E-cadherin-AF488, green; overlay in yellow) for untreated (control; upper panel) and RV16 treated (lower panel) and (**F**) showing the differentiated SAECs cell types including cilia (acetylated tubulin-AF647, magenta), goblet cells (MUC5AC-AF405, blue), club cells (SCGB3A2-AF555, red), and basal cells (cytokeratin 5-AF488, green), for the untreated (upper panel), RV16 treated (middle panel), and RV16 plus lipopolysaccharide (LPS) treated SAECs (lower panel). (**G**) Volcano plot of the up-regulated (red circles) and down-regulated (blue circles) genes comparing RV16 treated versus untreated SAECs as measured by Q-PCR. Labeled genes show at least a twofold change in expression at a significance level (α) of less than 0.05. (**H**) Heatmap of the significant differentially expressed genes for the RV16 treated SAECs ($n=5$) and untreated controls ($n=3$) showing low expression (green) and high expression (red) for the individual samples. Student's t-test, $^*p<0.05$, $^{**}p<0.01$, $^{***}p<0.001$, $^{****}p<0.0001$.

viral lower respiratory tract infection—were also associated with noticeably altered epithelial cilia formation (Fig. 3F). Other reports have similarly shown disappearance, fragmentation, or disordering of airway epithelial cilia in humans with acute rhinovirus infection[23,24] and in experimental models of severe acute respiratory syndrome coronavirus 2 (**SARS-CoV-2**) infection[25], which may impair mucociliary clearance and facilitate viral propagation in the airways.

We then assessed mRNA gene expression in the epithelial cells of the model using a targeted array. RV16 infection altered transcription of nine genes as measured by quantitative-PCR compared to untreated cells as shown in the volcano plot (Fig. 3G) and heatmap (Fig. 3H). RV16 increased transcription of the interferon response genes *interferon regulatory factor 7 (IRF7)*, *interferon alpha-inducible protein 6 (IFI6)*, *and interferon alpha-inducible protein 30 (IFI30)*; the interferon-inducible antiviral effector gene *guanylate-binding protein 1 (GBP1)*; the protein kinase gene *eukaryotic translation initiation factor 2 alpha kinase 2* (*EIF2AK2),* which is activated after binding to double stranded RNA; and the inflammatory genes *CXCL10*, *C–C motif ligand 2*

(CCL2), and *IL6*. Downregulation of the *caveolin-1 (CAV1)* gene was also noted, which controls airway epithelial barrier function[26] and regulates cilia length[27].

Validation of the model in experimental and clinical PARDS

We then treated with airway model with cytomix, a mixture of recombinant tumor necrosis factor alpha (TNF-α), interferon gamma (IFN-γ), and interleukin-1beta (IL-1β), which has been previously used in studies of lung injury as a surrogate for the inflammatory mediators in the pulmonary edema fluid of patients with acute respiratory distress syndrome[28,29]. Similar to the observations with RV16, cytomix also disrupted epithelial ZO-1 and E-cadherin in some areas, resulting in a decrease in the number of cell neighbors in affected cells (Fig. 4A). However, unlike RV16, cytomix did not disrupt cilia formation (Fig. 4B) or TEER at 4-h, 16-h, and 24-h exposure time points (Fig. 4C). Cytomix also increased CXCL10, CCL2, C–C motif ligand 3 (CCL3), IL-6, IL-17, and soluble receptor for advanced glycation end products (sRAGE) protein secretion on both the epithelial and endothelial sides of the model compared to sham or untreated cells (Fig. 4D–I).

Since cytomix induces a sterile lung injury that is not necessarily clinically relevant, we then pooled airway fluid from intubated children with mild (n = 10) and severe (n = 10) PARDS that was associated with respiratory viral infection. PARDS was defined by the Second Pediatric Acute Lung Injury Consensus Conference (PALICC-2) criteria, with severe PARDS defined by a sustained oxygen saturation index of at least 12 or an oxygenation index of at least 16 for a minimum of 4 h after initially meeting the diagnostic criteria for PARDS[4]. Endotracheal aspirate samples were collected within 24 h of intubation and processed within 30 min to yield cell free airway fluid supernatant. These endotracheal aspirate samples were thawed and pooled for experimentation. Features of the patient groups, which did not differ in key demographic features, are shown in Table 1. Like the observations with cytomix, airway fluid from children with severe PARDS reduced TEER (Fig. 5A) and significantly upregulated CXCL10, CCL2, CCL3, IL-6 IL-17, and sRAGE protein on the apical (epithelial) side of the model (Fig. 5B–G). CXCL10 and IL-6 protein also increased on the basal (endothelial) side of the model (Fig. 5B, E). These effects were driven by the cells in the model, since raw concentrations of these inflammatory mediators and the total protein content did not differ in the airway fluid of the pooled groups (Table 1).

Utility of the model for drug testing

Previous studies have demonstrated elevations of IL-6 in the airways of children with PARDS[17,30]. Recently, plasma IL-6 was also shown to be elevated in children with PARDS, particularly in those children with a "hyper-inflammatory" phenotype characterized by greater PARDS severity, a longer duration of mechanical ventilation, and higher mortality[31,32]. Since IL-6 signals through the STAT3 pathway, we examined the utility of the model for drug testing with baricitinib, which preferentially inhibits JAK1 and JAK2, thus inhibiting the effects of IL-6 on the STAT3 pathway[33–35]. When co-administered with cytomix, baricitinib significantly reduced both epithelial and endothelial IL-6 secretion (Fig. 6A, B). Baricitinib treatment also attenuated cytomix-induced proliferation of basal cells and club cells, which function as progenitor cells during airway insults to repair epithelial barrier defects (Fig. 6C, first and second columns, respectively). Phosphorylation of STAT3 was increased in cytomix treated SAECs (mean ± standard deviation [SD] maximal projection intensity: 132 ± 31) compared to untreated SAECs (mean ± SD maximal projection intensity: 110 ± 32) (Fig. 6C, third column). Baricitinib attenuated STAT3 phosphorylation in the presence of cytomix compared to cytomix treated SAECs (mean ± SD maximal projection intensity: 82 ± 29) (Fig. 6C, third column). STAT3 expression also appeared less in baricitinib + cytomix treated SAECs compared to untreated and cytomix treated cells (Fig. 6C, fourth column).

Discussion

Inflammation and the loss of alveolar epithelial and lung vascular endothelial permeability barriers are some of the hallmark features of pediatric acute respiratory distress syndrome pathobiology[2,3]. While plasma biomarkers, cultured alveolar epithelial cells, and preclinical animal models help us better understand the underlying pathobiology of PARDS, there is no single biomarker, cell culture, or animal model that replicates the complex pathobiology and captures the inherent heterogeneity of PARDS in humans[7,11]. Human-based preclinical models used in combination with patient biospecimens allow for hypothesis testing of molecular mechanisms of PARDS. Furthermore, such preclinical models could assist with in vitro drug candidate screening and testing to link clinical subphenotypes with endotypes in PARDS. In this study, we developed a human-based preclinical model using primary small airway epithelial cells and human umbilical vein endothelial cells (SAEC/HUVECs) cultured at the air–liquid interface for use in understanding the molecular mechanisms in acute lung injury. Because lower respiratory tract viral infections and bacterial pneumonias are the most frequent triggers of PARDS[1,4], we demonstrated the clinical relevance of our model by showing that the epithelial and endothelial cytokine response to both a human rhinovirus infection and a proinflammatory cytokine cocktail elicit a similar proinflammatory cytokine response as compared to that of endotracheal aspirates of children with severe PARDS. We then illustrate the utility of the SAEC/HUVECs model in drug testing by showing the reduction in IL-6 and STAT3 phosphorylation following co-treatment of SAECs with cytomix and the Janus kinase (JAK) inhibitor baricitinib.

The epithelium can be directly injured by viruses, bacterial endotoxins, acid, hyperoxia, hypoxia, mechanical forces, and by inflammatory cells or their byproducts[3]. In addition to disruption of the alveolar epithelial (type I and type II cells) and pulmonary vascular endothelial barriers, small airway dysfunction also commonly occurs in patients with ARDS[36–38]. Small airway epithelial cells conducts air to and from the alveoli, and is composed of columnar and cuboidal cells. The major small airway epithelial cell types include ciliated, goblet, club, and basal cells. Goblet and ciliated cells are responsible for mucus production and mucociliary clearance of inhaled pathogens and particles from the environment. In addition to being the first line barrier against inhaled

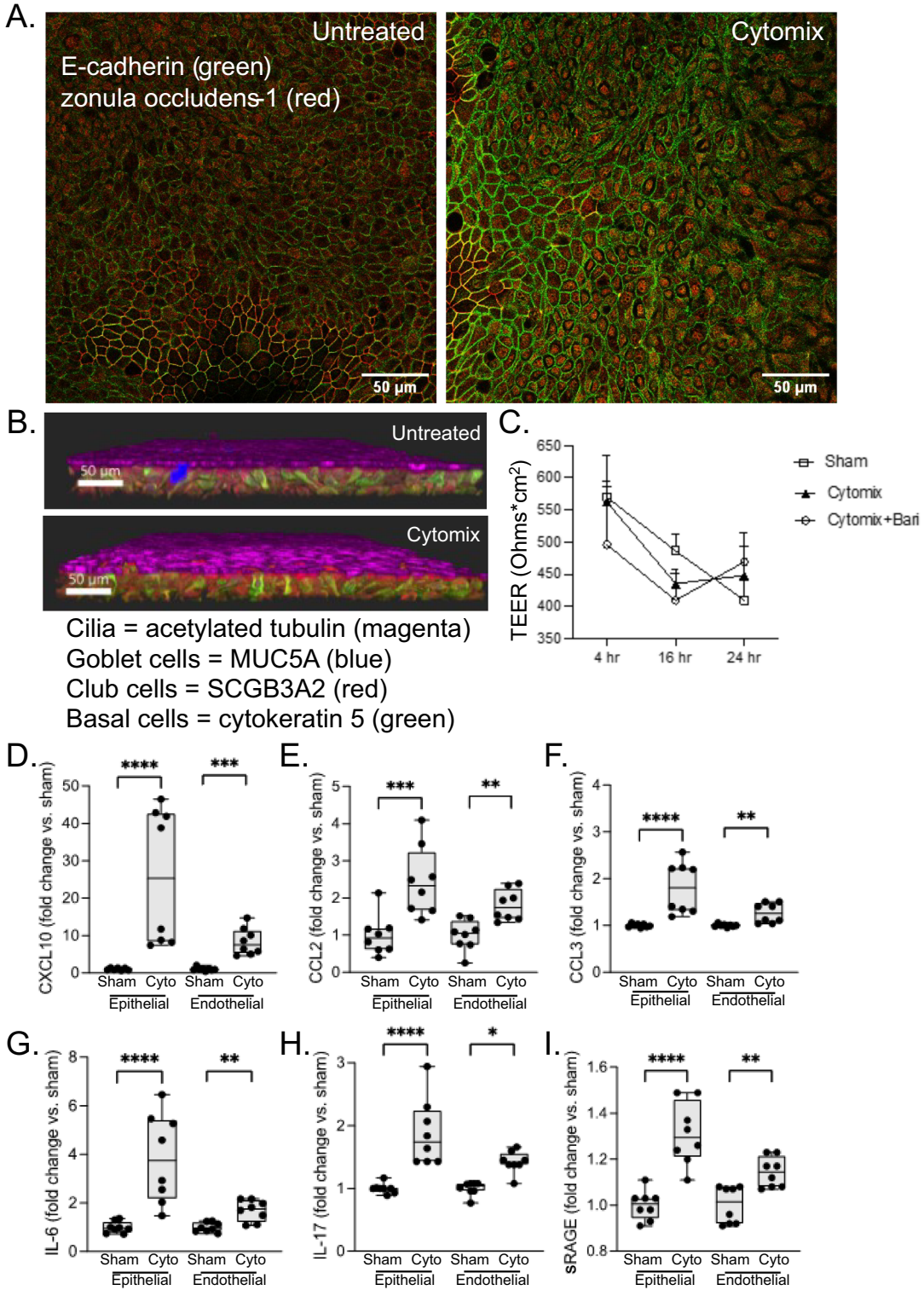

pathogens and particles, the airway epithelium also participates in immune defense to control inflammation[39]. Recently, lung tissue from adult patients with ARDS was examined to quantify structural and functional changes in small airway epithelium[36]. Similar to the findings following RV16 infection in our model, the airways of ARDS had increased epithelial denudation with a loss of ciliated cells and increased epithelial permeability indicated by a decrease in tight junction and adherens junction proteins[36]. In a reconstructed human bronchial epithelium model infected with SARS-CoV-2, tight junctions were disrupted resulting in a transient decrease in epithelial barrier function and rapid, extensive loss of cilia leading to poor mucociliary clearance[25]. Moreover, quantitative image analysis of SARS-CoV-2 infected human bronchial epithelium showed that there were fewer neighbors per cell compared to the mock infected bronchial epithelium indicating active epithelial remodeling[25]. RV16 infection in the SAEC/UVEC model also disrupted the structure of the epithelial layer and elicited strong innate immune and anti-viral responses at the gene transcript and protein level.

◀**Fig. 4**. Exposure of the small airway epithelial cells (SAECs) in the model to cytomix (10 ng/ml each of tumor necrosis factor alpha [TNF-α], interferon gamma [IFN-γ], and interleukin-1 beta [IL-1β]). Confocal immunofluorescence microscopy images visualized using LASX 3D Viewer, of tight junctions (zonula occludens-1-AF647, red; E-cadherin-AF488, green) for untreated (control; left panel) and cytomix treated (right panel) and (**B**) showing the differentiated SAECs cell types including cilia (acetylated tubulin-AF647, magenta), goblet cells (MUC5AC-AF405, blue), club cells (SCGB3A2-AF555, red), and basal cells (cytokeratin 5-AF488, green) for the untreated (upper panel), cytomix treated SAECs (lower panel). (**C**) Transepithelial electrical resistance (Ω^*cm^2) in untreated (control) and cytomix treated SAECs. Fold change in cytokine expression of SAECs following cytomix treatment compared to untreated control for (**D**) C–X–C motif chemokine ligand 10 (CXCL10), (**E**) C–C motif ligand 2 (CCL2), (**F**) C–C motif ligand 3 (CCL3), (**G**) interleukin-6 (IL-6), (**H**) IL-17, and (**I**) soluble receptor for advanced glycation end products (sRAGE) for 2 independent experiments with 4 replicates per experiment. Student's t-test, $^*p<0.05$, $^{**}p<0.01$, $^{***}p<0.001$, $^{****}p<0.0001$.

Feature	Mild PARDS N = 10	Severe PARDS N = 10	*p*-value
Age (months)	7 (2, 21)	14 (1, 25)	0.239[b]
Sex (Male/Female)	8/2	5/5	0.160[a]
Ethnicity (Hispanic/Not Hispanic)	1/9	1/9	1.000[a]
Race (White/Black/Multiple)	4/6/0	4/4/2	0.301[a]
PRISM score	12 (8, 18)	20 (4, 27)	0.129[b]
PELOD score	7 (4, 12)	9.5 (3, 14)	0.219[b]
PICU admission days	7 (3, 9)	14 (6, 36)	0.008[b]
Ventilator days	5 (3, 8)	13 (2, 34)	0.003[b]
Viral Respiratory Panel Performed* Virus not identified Single virus identified Multiple viruses detected RSV detected Rhinovirus/enterovirus detected Influenza A or B detected HMPV detected Adenovirus detected Parainfluenza detected Coronavirus detected	9 1 4 4 3 5[c] 1 0 0 0 3	9 1 6 2 3 3[d] 1 1 1 1 0	1.000[a] 1.000[a] 0.302[a] 0.302[a] 1.000[a] 0.343[a] 1.000[a] 0.303[a] 0.303[a] 0.303[a] 0.303[a]
Positive Bacterial Culture	7	8	0.606[a]
Airway fluid constituents Total protein (ng/mL) CCL3 (pg/mL) IL-6 (pg/mL) IL-17 (pg/mL) RAGE (pg/mL)	1.6 (0.3, 3.5) 145 (23, 459) 247 (8, 425) 6 (2, 9) 49 (3, 178)	0.5, (0.1, 5.9) 49 (3, 463) 46 (1, 1075) 5 (1, 22) 33 (3, 755)	0.901[b] 0.401[b] 0.804[b] 0.835[b] 0.345[b]

Table 1. Features of the participants with PARDS. Data are shown as the median (minimum, maximum), unless otherwise indicated. *P*-values were assessed with [a]Chi-square and [b]Mann Whitney U tests. *Viruses are not mutually exclusive – some patients are co-infected. [c]One child in the Mild PARDS group had a single virus detected that was Rhinovirus/enterovirus. [d]Two children in the Severe PARDS group has a single virus detected that was Rhinovirus/enterovirus.

Notably, the gene for *caveolin-1* (*CAV-1*) was down-regulated in RV16 infected SAECs. CAV-1 helps to maintain both epithelial and endothelial barrier integrity through regulation of tight junctions[40]. CAV-1 is the main protein component of caveolae which are involved in transmembrane transport, endocytosis, lipid metabolism, and signal transduction[41]. In primary newborn rat type II alveolar epithelial cells (AECII), CAV-1 knockdown by silencing RNA reduced the expression of tight junction proteins ZO-1, occludin, and claudin-4, and disrupted the pulmonary epithelial barrier integrity under normoxic conditions[42]. However, in an LPS-induced mouse model of acute lung injury, knockdown of CAV-1 mitigated acute lung injury through the reduced activation of NF-κB, reduced inflammatory cell infiltration into the lung, and a decreased inflammatory cytokine response[41,43]. Inhibition of the CAV-1/NF-κB axis activated autophagy via inhibition of AKT/mTOR signaling and activation of AMPK signaling[41]. Deletion of CAV-1 in mice has also been shown to upregulate cytoprotective genes such as hemeoxygenase (HO-1) and survinin resulting in reduced epithelial cell apoptosis following hyperoxia exposure[44–47]. Thus, the significance of the down-regulation of *CAV*-1 in our model appears more in line with tight junction disruption and epithelial barrier integrity under normoxic conditions as previously shown in the newborn rat AECII model; however, future work could explore the role of CAV-1 in response to viral and cytomix stimuli.

Soon after a clinical insult triggering the inflammatory pathways leading to PARDS, high levels of the proinflammatory cytokines TNF-α, IL-1β, IL-8, and TGF-β1 are found in the lung edema fluid from patients with ARDS[17,48–51]. Cytomix is a mixture of three proinflammatory cytokines, TNF-α, IL-1β, and IFN-γ, that serves as

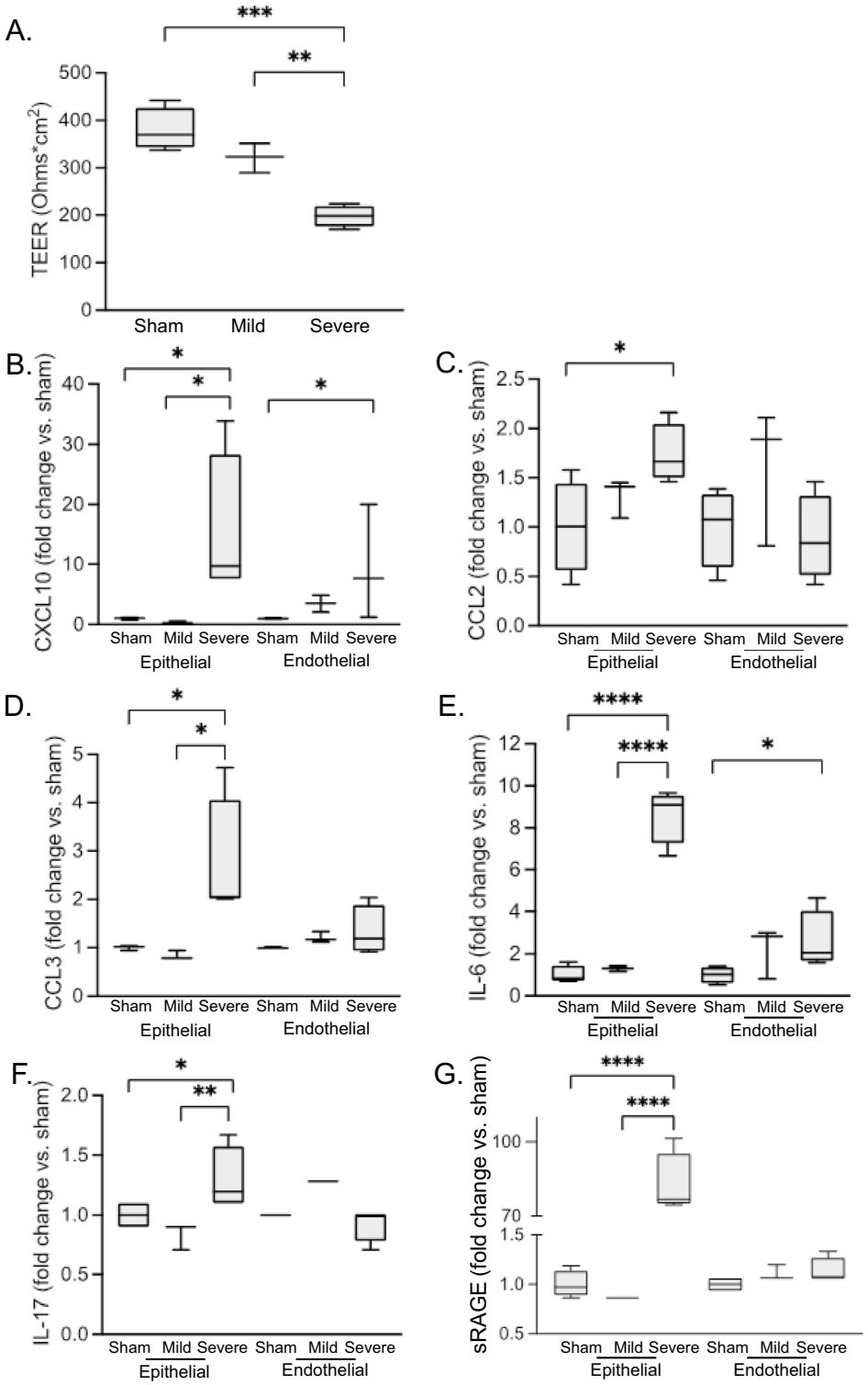

Fig. 5. Exposure of the small airway epithelial cells (SAECs) in the model to pooled endotracheal aspirates (TA) from children with mild ($n = 10$) and severe ($n = 10$) pediatric acute respiratory distress syndrome (PARDS) samples. (**A**) Transepithelial electrical resistance (Ω^*cm^2) in untreated (sham), mild PARDS TA, and severe PARDS TA treated SAECs. Fold change in cytokine expression from the epithelial (apical side) and endothelial (basal side) following mild and severe PARDS TA treatment compared to untreated (sham) SAECs for (**B**) C–X–C motif chemokine ligand 10 (CXCL10), (**C**) C–C motif ligand 2 (CCL2), (**D**) C–C motif ligand 3 (CCL3), (**E**) interleukin-6 (IL-6), (**F**) IL-17, and (**G**) soluble receptor for advanced glycation end products (sRAGE) One-way ANOVA with *post-hoc* Tukey test. $^*p < 0.05$, $^{**}p < 0.01$, $^{***}p < 0.001$, $^{****}p < 0.0001$. Experiments were performed twice with three–four biological replicates per experiment.

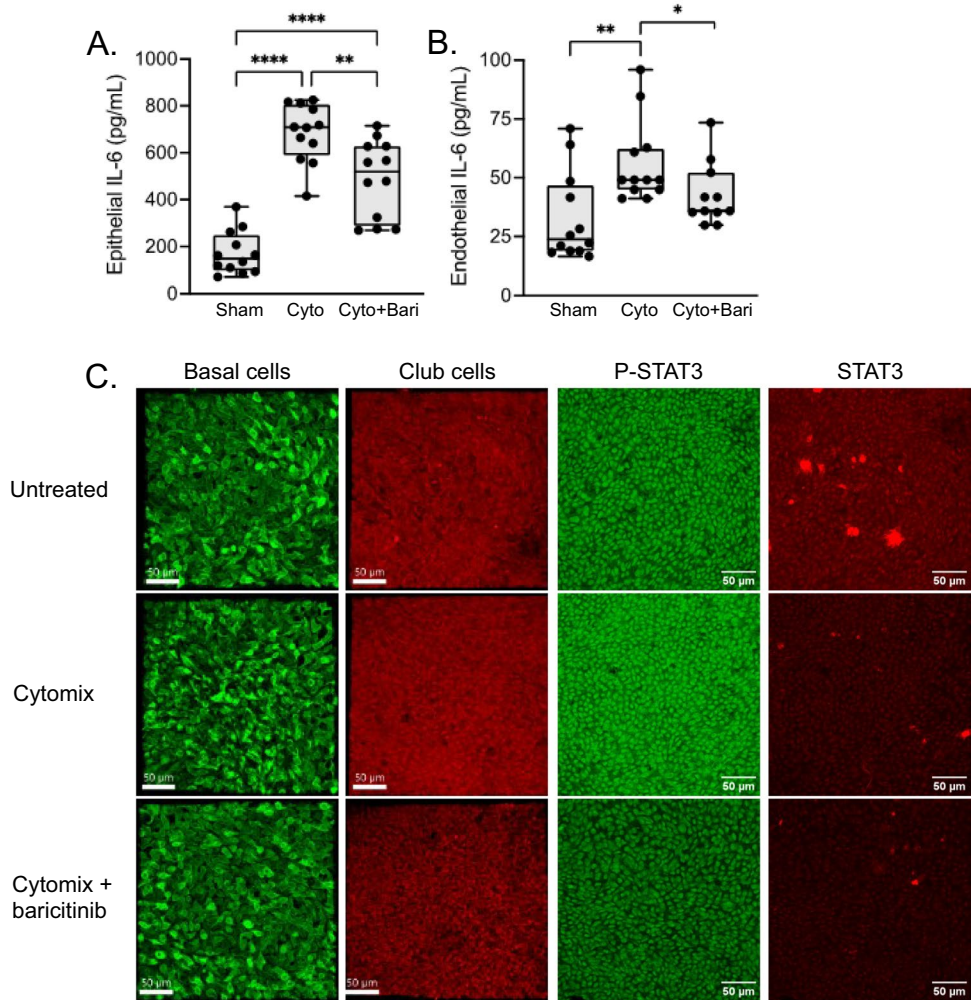

Fig. 6. Drug testing using the small airway epithelial cell (SAEC)/human umbilical vein endothelial cell (HUVEC) model with cytomix as the inflammatory exposure. Measurement of (**A**) SAEC (epithelial) and (**B**) HUVECs (endothelial) expression of interleukin-6 (IL-6; pg/ml) in response to untreated (sham), cytomix (10 ng/ml each of tumor necrosis factor alpha [TNF-α], interferon gamma [IFN-γ], and interleukin-1 beta [IL-1β]), and cytomix plus the JAK1/2 inhibitor baricitinib (1 µM) for 24 h at 37 °C, 5% CO_2. Independent experiments (n = 2), replicates per experiment (n = 6). $^{*}p < 0.05$, $^{**}p < 0.01$, $^{***}p < 0.001$, $^{****}p < 0.0001$. Confocal immunofluorescence microscopy images (**C**) showing basal cells (cytokeratin 5-AF488, green; left panels), club cells (SCGB3A2-AF555, red; right panels) and pSTAT3 (green) and STAT3 (red) expression in SAECs for the untreated (top panels), cytomix (middle panels), and cytomix plus baricitinib treated (lower panels) SAECs. Images were taken at the same laser intensity for untreated, cytomix and cytomix + baricitinib treated samples.

an established model for the pulmonary edema fluid in ARDS[48,52]. In our SAEC/HUVEC model, cytomix evoked a high levels of proinflammation cytokines IL-6, IL-17, CCL2, CCL3, CXCL10, and sRAGE from both the apical (epithelial) and basal (endothelial) sides of the model. These findings are consistent with other studies whereby CCL2 protein levels are elevated in the bronchoalveolar fluid from LPS-challenged human volunteers and in patients with ARDS[53]. Like CCL2 which promotes neutrophil migration into the airways of patients with ARDS, CCL3 is a chemokine that facilitates recruitment of leukocytes to the lung resulting in capillary leak and early mortality in mice exposed to LPS[54,55]. CXCL10 is another chemokine that controls neutrophil recruitment to the lungs resulting in severe inflammation including the release of inflammatory mediators IL-6, IFN-γ, and ICAM-1, in experimental ARDS[56–58]. In patients with COVID-19 induced ARDS, an uncontrolled innate and impaired adaptive immune response with a "chemokine signature" characterized by elevated serum concentrations of CXCL10 and GM-CSF were associated with higher mortality at 28-days[59]. sRAGE is another known marker of alveolar epithelial type I cell injury in acute lung injury, and is associated with impaired alveolar fluid clearance, increased severity of lung injury, and higher mortality[60–63]. We further validated our model by treating the SAEC (apical) side with airway fluid obtained from endotracheal aspirates of intubated children with mild and severe PARDS. We show that the airway fluid from children with severe PARDS resulted in barrier disruption (lower TEER, disrupted tight junctions) and secretion of pro-inflammatory cytokines on both the epithelial and endothelial side of the model (elevated CCL2, CCL3, IL6, sRAGE, and CCL10) compared to treatment with mild

PARDS or untreated (control). Although only the SAEC side was exposed to airway fluid, crosstalk between the SAEC and HUVEC cells occurred as shown by the proinflammatory cytokine response by the endothelial cells on the basal side of the model. Thus, the SAEC/HUVEC model herein described recapitulates many of the inflammatory features seen in patients with ARDS.

Baricitinib is a selective Janus kinase (JAK)1/JAK2 inhibitor approved for the treatment of hospitalized adults with COVID-19 ARDS[13,14,64,65]. Baricitinib inhibits STAT3 phosphorylation and reduces multiple hyperinflammatory cytokines including IL-1β, TNF-α, and IL-6 that are biomarkers implicated in COVID-19 pneumonia and ARDS pathobiology[66]. Several randomized controlled trials conducted during the COVID-19 pandemic and a meta-analysis showed that treatment with a JAK inhibitor—primarily baricitinib—reduced mortality in patients hospitalized for COVID-19 by about 20%[12,13,65]. Therefore, we tested the SAEC and HUVEC response to cytomix with and without co-culture with baricitinib. In response to cytomix, both basal and club cells seemed to proliferate compared to the untreated controls. Treatment of the SAEC with baricitinib in the presence of cytomix resulted in a reduced levels of epithelial and endothelial IL-6 expression levels due to inhibition of STAT-3 phosphorylation. Furthermore, basal and club cell proliferation was decreased in the cytomix stimulated group treated with baricitinib similar to the levels seen in the untreated (control) when compared to the cytomix-stimulated group.

One explanation for the basal and club cell proliferation seen in the SAEC/HUVEC model in response to cytomix stimulation is that basal cells are the main stem cells of the small airway epithelium with the ability to self-renew following injury. Basal cells can differentiate into most other important cell types including goblet, club and ciliated cells, among others in the airway epithelium[67]. Similar to basal cells, club cells also have stem cell properties and can participate in epithelial repair by differentiating into both ciliated and goblet cells[67–69]. Club cells can also dedifferentiate into basal cells upon basal cell injury and loss[67–69]. Club cells maintain homeostasis in the lung and one of their secreted proteins, Clara Cell Secretory Protein (CC16), has anti-inflammatory and immunosuppressive abilities through inhibition of IFN-γ, TNF-α, and IL-1β production by leukocytes and the inhibition of neutrophil and monocyte recruitment and phagocytic function[67,70–72]. In SARS-CoV-2 infection, basal cells have been shown to mobilize following damage to ciliated cells[25]. Thus, our model shows similar response properties to an immunomodulatory drug approved for use in adults with severe and critical COVID-19 pneumonia and ARDS.

A potential contributing mechanism that future work may investigate is whether cytomix causes a proliferative arrest in the SAEC cells via the STAT/IRF1 axis to promote a senescent associated secretory phenotype as seen in alveolar A549 cells exposed to IFN-γ and TNF-α[73]. Recent work has shown that baricitinib prevented IFN-γ and TNF-α induced alveolar epithelial cell growth arrest and the induction of the SASP through inhibition of STAT1 phosphorylation[73]. The exposure of rhinovirus, cytomix, or airway tracheal aspiratory fluid was performed on the SAEC (airway side) of the model and thus we cannot comment on the direct effects of rhinovirus, cytomix, or airway tracheal aspiratory fluid on the endothelial side of the model. Future work to investigate the effects of cytomix or patient plasma on the endothelial (basal) side of the model can be performed with HUVECs or primary human lung microvascular endothelial cells (HMVECs) as an indirect trigger of acute lung inflammation. Finally, we chose to use SAEC in our model; however, co-cultures of AECI and AECII cells to mimic the alveolar-capillary space could also be used in future model iterations.

In summary, we show the physiologic relevance of a SAEC/HUVECs model to study mechanisms of PARDS using both a rhinovirus and cytomix airway epithelial insult. We further highlight the use of the model to test baricitinib, a JAK1/JAK2 inhibitor approved to treat COVID-19 pneumonia and ARDS, to reduce epithelial production of IL6. We conclude that this model system is useful for the study of PARDS pathobiology and may provide a high throughput option for novel drug candidate testing for treatment of PARDS in children.

Methods

Culture of primary human airway epithelial cells

Primary human small airway epithelial cells (**SAECs**) isolated from normal human lung tissue in the distal portion of the lung (bronchiole area 1 mm) were purchased from Lonza (Basel, Switzerland) and expanded in PneumaCult-Ex Plus Media (StemCell Technologies, Vancouver, BC, Canada) in 75 cm^2 tissue culture flasks until 85% confluency. Cells were harvested with Animal Component-Free Cell Dissociation Kit (Stem Cell Technologies, Vancouver, BC) and plated on 6.5-mm Transwell 0.4-µm Pore Polyester membrane inserts (Corning, Lowell, Mass) at a density of 2×10^5 cells/cm^2 and incubated at 37 °C, 5% CO_2 until confluent, for approximately 3–4 days. Once confluent, cells were transitioned and maintained at air–liquid interface culture with PnuemaCult-ALI-S Maintenance Medium (StemCell Technologies) at 37 °C, 5% CO_2 as per the manufacturer's instructions for 28 days until fully differentiated.

Culture of human vascular endothelial cells (HUVECs)

Primary Umbilical Vein Endothelial cells were purchased from ATCC and cultured to 90% confluency using ATCC's Endothelial Cell Growth Kit—VEGF. Cells were harvested using with Animal Component-Free Cell Dissociation Kit (Stem Cell Technologies) and plated on the underside of differentiated transwells.

RV16 culture

H1 HELA cells were purchased from ATCC grown at 37 °C, 5%CO_2 to confluency in L-15 media supplemented with 10% Fetal Bovine Serum. Once confluent cells were infected with Human rhinovirus 16 Strain 11,757 (RV16) in EMEM with 2% FBS at 33 °C and 5% CO_2 for 2 h with gentle rocking every 15 min. After 2 h additional media was added and cells allowed to incubate for 3 days. Cells and media were harvested, sonicated and centrifuged to remove cells and debris. The remaining supernatant was placed in 1 ml aliquots, snap frozen

and stored in liquid nitrogen. A standard plaque asssy was used to determine Pfus/ml of virus stock. A MOI of 10 was used for all experiments.

Cellular imaging

Epithelial cells and endothelial cells were visualized by inverted confocal microscopy (Stellaris 8, Leica, Deerfield, Ill) and Imaris imaging software version 10.0 (Oxford Instruments, Abingdon, United Kingdom). Epithelial cell types were stained with MUC5AC-AF405 (1:200; Novus Biologicals, Centennial, Colo), SCGB3A2-AF555 (1:100; Abcam, Fremont, Calif), cytokeratin 5-AF488 (1:200; Abcam), and acetylated-tubulin-AF647 (1:100; Santa Cruz Biotechnology, Dallas, Tex) and tight junctions were stained with zonula occludens-1-AF647 (1:50, Cell Signaling Technology, Danver, MA) and E-cadherin-AF488 (1:50, Cell Signaling Technology, Danver, MA). HUVECs were stained with VE-cadherin-AF594 (1:50, Biolegend, San Diego, CA). Stat3 (D3Z2G) Rabbit mAb (Alexa Fluor® 488 Conjugate) and Phospho-Stat3 (Tyr705) (D3A7) XP® Rabbit mAb (Alexa Fluor® 555 Conjugate) were used at 1:50 dilution (Cell Signaling Technology, Danvers, MA, USA). Fluorescence intensity for p-STAT3 was quantified using ImageJ by taking a maximal intensity projection (Image ▼ Stacks ▼ Z project). The options for Z project are: "Start slice 1, Stop slice 133, Projection type = Max intensity"). The mean and standard deviation of the maximal intensity projection are then reported using the menu option Analyze ▼ Measure in a new window.

CytoMix treatments

To formulate Cytomix media, recombinant human TNF-α, IL-1β, and IFN-γ (Peprotech, Cranbury, NJ) were added to EMEM without FBS to a final concentration of 50 ng/ml each. Cytomix media was placed on the apical side of treated wells for the indicated time period. Baricitinib was added to cytomix media for a final concentration of 1 μg/ml, as noted.

Transepithelial electrical resistance (TEER)

Integrity of tight junctions were assessed using a EVOM2 Voltohmmeter (World Precision Instruments, Sarasota, FL) equipped with sterilized STX2 chopstick. Measurements were taken using ALI-3 media on both the apical and basal sides of the chamber.

Cytokine measurement

Cytokines were measured from the conditioned media collected following SAEC exposure to rhinovirus, cytomix, or patient pooled endotracheal aspirate from both the apical (epithelial) side and the basal (endothelial) side of the transwell using xMap technology, specifically: Milliplex Human Sepsis Panel 1 kit (Millipore, Burlington, MA), Milliplex Human Cytokine/Chemokine/Growth Factor Panel A (Millipore) and Human Luminex Discovery Assay (R&D System's, Minneapolis, MN).

Quantitative PCR

Sham or RV16 treated Small Airway Epithelial Cells (SAECs) were harvested via physical manipulation from trans-well membranes and immediately preserved in RNAlater (Sigma, St. Louis, MO). Total RNA was purified using the NucleoSpin RNA PLUS kit (Takara Bio USA, Inc., San Jose, CA) per manufacturer's instructions. Sample RNA was processed to yield cDNA and pre-amplified using RT^2-PreAMP cDNA Synthesis Kit with the appropriate Pathway Primer Mix (Qiagen, Hilden, Germany). Pre-amplified samples were then evaluated using RT^2 Profiler™ PCR Array Human Type I Interferon Response Array (Qiagen, Hilden, Germany) per the manufacturer's instructions. Change in Ct values were calculated and relative expression of target genes reported. The average Ct values of the following housekeeping genes used to normalize the differential gene expression included actin (ACTB), beta-2-microglobulin (B2M), glyceraldehyde-3-phosphate dehydrogenase (GAPDH), hypoxanthine phosphoribosyltransferase 1 (HPRT1), and ribosomal protein, large, P0 (RPLP0).

Patient cohort, sample collection and processing

Children older than 14 days with a corrected gestational age of 37 weeks and younger than 17 years who were endotracheally intubated for less than 72 h were eligible for participation as approved by the Emory University Institutional Review Board (IRB00113035) according to the principles of the Declaration of Helsinki. Informed consent from a parent or legal guardian was obtained for study participation and prior to performing any study procedures. Children were excluded if they had any of the following: perinatal related lung disease, respiratory failure fully explained by cardiac failure or fluid overload, chronic respiratory failure requiring mechanical ventilation via a tracheostomy, a baseline oxygen requirement of 2 L of oxygen or greater at home, a specific order not to preform airway clearance, a history of excessive bleeding or a known bleeding disorder or through to be at high risk of bleeding by clinical team, an airway surgical procedure below the level of the endotracheal tube, a do not resuscitate or a limited resuscitation order, child was a ward of the state or there were no available legal parents or guardians from whom to obtain informed consent, or an attending physician did not wish for the patient to participate in the study. PARDS and severity stratification were performed at the time of sample collection according to the 2023 Second Pediatric Acute Lung Injury Consensus Conference (PALICC-2) criteria[4,74]. The Pediatric Risk of Mortality-III was calculated at the time of PICU admission[75]. The Pediatric Logistic Organ Dysfunction-2 score was calculated within 24 h of study enrollment[76].

Endotracheal aspirates were collected within 72 h of intubation by instilling up to 5 mL of sterile saline into the endotracheal tube using the inline Ballard suction catheter into a sterile Lukens trap. A repeat passage of the Ballard catheter was performed if less than half of the instilled volume was not returned. Additional saline was used to flush the aspirate into the Lukens trap. The airway fluid was separated from the cells by centrifugation at 800 × *g* for 15 min at 4 °C. Airway fluid supernatant was collected into a fresh tube, centrifuged at 3000 × *g*

for 15 min at 4 °C to remove any remaining cells and debris, and was stored at − 80 °C until use. Separate pools of airway fluid from ten participants with mild/moderate PARDS and ten participants with severe PARDS were used in model experiments.

Statistical analyses

Descriptive statistics were used to summarize the demographic and clinical features using the median (minimum, maximum) for continuous variables and count (percent) for categorical variables. Differences between the two group for the demographic and clinical features were assessed using the Mann Whitney U test for non-normal distributions of continuous variables and a chi-square test for categorical variables. Cytokine data generated in the SAEC/HUVECs model was summarized as fold-change using the sham group as the reference. A Student's t-test was used to test for differences between two groups. A one-way analysis of variance (ANOVA) with a *post-hoc* Tukey test was used for multiple comparisons. A *p*-value of less than 0.05 was the threshold for statistical significant. Data were analyzed with IBM SPSS Statistics (Version 24.0) and GraphPad Prism 10 (Version 10.4.1).

Data availability

The datasets generated during and/or analyzed during the current study are available from the corresponding author on reasonable request.

Received: 15 January 2025; Accepted: 12 May 2025
Published online: 21 May 2025

References

1. Khemani, R. G. et al. Paediatric acute respiratory distress syndrome incidence and epidemiology (PARDIE): An international, observational study. *Lancet Respir. Med.* **7**, 115–128. https://doi.org/10.1016/S2213-2600(18)30344-8 (2019).
2. Grunwell, J. R. et al. Pathobiology, severity, and risk stratification of pediatric acute respiratory distress syndrome: From the second pediatric acute lung injury consensus conference. *Pediatr. Crit. Care Med.* **24**, S12–S27. https://doi.org/10.1097/PCC.0000000000003156 (2023).
3. Matthay, M. A. et al. Acute respiratory distress syndrome. *Nat. Rev. Dis. Primers* **5**, 18. https://doi.org/10.1038/s41572-019-0069-0 (2019).
4. Yehya, N. et al. Definition, incidence, and epidemiology of pediatric acute respiratory distress syndrome: From the second pediatric acute lung injury consensus conference. *Pediatr. Crit. Care Med.* **24**, S87–S98. https://doi.org/10.1097/PCC.0000000000003161 (2023).
5. Kneyber, M. C. J. et al. Understanding clinical and biological heterogeneity to advance precision medicine in paediatric acute respiratory distress syndrome. *Lancet Respir. Med.* **11**, 197–212. https://doi.org/10.1016/S2213-2600(22)00483-0 (2023).
6. Orwoll, B. E. & Sapru, A. Biomarkers in pediatric ARDS: Future directions. *Front Pediatr.* **4**, 55. https://doi.org/10.3389/fped.2016.00055 (2016).
7. Carlton, E. F. & Flori, H. R. Biomarkers in pediatric acute respiratory distress syndrome. *Ann. Transl. Med.* **7**, 505. https://doi.org/10.21037/atm.2019.09.29 (2019).
8. Whitney, J. E. et al. Endothelial biomarkers are associated with indirect lung injury in sepsis-associated pediatric acute respiratory distress syndrome. *Crit. Care Explor.* **2**, e0295. https://doi.org/10.1097/CCE.0000000000000295 (2020).
9. Sathe, N. A. et al. Alveolar biomarker profiles in subphenotypes of the acute respiratory distress syndrome. *Crit. Care Med.* **51**, e13–e18. https://doi.org/10.1097/CCM.0000000000005704 (2023).
10. Williams, J. G. et al. Comparison of sixteen pediatric ARDS-associated plasma biomarkers with changing lung injury severity. *Pediatr. Crit. Care Med.* **25**, e31–e40 (2023).
11. Zalucky, A. A., Matthay, M. A. & Ware, L. B. Biomarkers of acute respiratory distress syndrome: Current state and future prospects. *Clin. Chest Med.* **45**, 809–820. https://doi.org/10.1016/j.ccm.2024.08.003 (2024).
12. Group, R. C. Baricitinib in patients admitted to hospital with COVID-19 (RECOVERY): A randomised, controlled, open-label, platform trial and updated meta-analysis. *Lancet* **400**, 359–368. https://doi.org/10.1016/S0140-6736(22)01109-6 (2022).
13. Kalil, A. C. et al. Baricitinib plus remdesivir for hospitalized adults with Covid-19. *N. Engl. J. Med.* **384**, 795–807. https://doi.org/10.1056/NEJMoa2031994 (2021).
14. Marconi, V. C. et al. Efficacy and safety of baricitinib for the treatment of hospitalised adults with COVID-19 (COV-BARRIER): A randomised, double-blind, parallel-group, placebo-controlled phase 3 trial. *Lancet Respir. Med.* **9**, 1407–1418. https://doi.org/10.1016/S2213-2600(21)00331-3 (2021).
15. Srinivasan, B. et al. TEER measurement techniques for in vitro barrier model systems. *J. Lab. Autom.* **20**, 107–126. https://doi.org/10.1177/2211068214561025 (2015).
16. Grunwell, J. R. et al. RNA sequencing analysis of monocytes exposed to airway fluid from children with pediatric acute respiratory distress syndrome. *Crit. Care Explor.* **6**, e1125. https://doi.org/10.1097/CCE.0000000000001125 (2024).
17. Ripple, M. J., Mohammad, A. F., Stephenson, S. T., Fitzpatrick, A. M. & Grunwell, J. R. Expression patterns of airway fluid cytokines from intubated children with pediatric acute respiratory distress syndrome. *Crit. Care Explor.* **4**, e0819. https://doi.org/10.1097/CCE.0000000000000819 (2022).
18. Jackson, D. J. et al. Wheezing rhinovirus illnesses in early life predict asthma development in high-risk children. *Am. J. Respir. Crit. Care Med.* **178**, 667–672. https://doi.org/10.1164/rccm.200802-309OC (2008).
19. Yang, Z., Mitlander, H., Vuorinen, T. & Finotto, S. Mechanism of rhinovirus immunity and asthma. *Front Immunol.* **12**, 731846. https://doi.org/10.3389/fimmu.2021.731846 (2021).
20. Schworer, S. A. et al. IL-1 receptor antagonist attenuates proinflammatory responses to rhinovirus in airway epithelium. *J. Allergy Clin. Immunol.* **151**, 1577–1584. https://doi.org/10.1016/j.jaci.2023.01.015 (2023).
21. Nakagome, K. & Nagata, M. Innate immune responses by respiratory viruses, including rhinovirus. during asthma exacerbation. *Front Immunol.* **13**, 865973. https://doi.org/10.3389/fimmu.2022.865973 (2022).
22. Zhu, Z. et al. Rhinovirus stimulation of interleukin-6 in vivo and in vitro. Evidence for nuclear factor kappa B-dependent transcriptional activation. *J. Clin. Invest.* **97**, 421–430. https://doi.org/10.1172/JCI118431 (1996).
23. Martinez-Giron, R., Van Woerden, H. C. & Martinez-Torre, C. Ciliated nasal epithelial cells damage and human rhinovirus infection: cytological findings. *Acta Biomed.* **91**, 146–147. https://doi.org/10.23750/abm.v91i1.8924 (2020).
24. Basnet, S. et al. Rhinovirus C causes heterogeneous infection and gene expression in airway epithelial cell subsets. *Mucosal Immunol.* **16**, 386–398. https://doi.org/10.1016/j.mucimm.2023.01.008 (2023).
25. Robinot, R. et al. SARS-CoV-2 infection induces the dedifferentiation of multiciliated cells and impairs mucociliary clearance. *Nat. Commun.* **12**, 4354. https://doi.org/10.1038/s41467-021-24521-x (2021).

26. Hackett, T. L. et al. Caveolin-1 controls airway epithelial barrier function. Implications for asthma. *Am. J. Respir. Cell Mol. Biol.* **49**, 662–671. https://doi.org/10.1165/rcmb.2013-0124OC (2013).
27. Rangel, L. et al. Caveolin-1alpha regulates primary cilium length by controlling RhoA GTPase activity. *Sci. Rep.* **9**, 1116. https://doi.org/10.1038/s41598-018-38020-5 (2019).
28. Zhai, R. et al. Effects of sevoflurane on lung epithelial permeability in experimental models of acute respiratory distress syndrome. *J. Transl. Med.* **21**, 397. https://doi.org/10.1186/s12967-023-04253-w (2023).
29. Schwede, M. et al. Effects of bone marrow-derived mesenchymal stromal cells on gene expression in human alveolar type II cells exposed to TNF-alpha, IL-1beta, and IFN-gamma. *Physiol. Rep.* **6**, e13831. https://doi.org/10.14814/phy2.13831 (2018).
30. Wong, J. J. M. et al. Large scale cytokine profiling uncovers elevated IL12-p70 and IL-17A in severe pediatric acute respiratory distress syndrome. *Sci. Rep.* **11**, 14158. https://doi.org/10.1038/s41598-021-93705-8 (2021).
31. Dahmer, M. K. et al. Identification of phenotypes in paediatric patients with acute respiratory distress syndrome: A latent class analysis. *Lancet Respir. Med.* **10**, 289–297. https://doi.org/10.1016/S2213-2600(21)00382-9 (2022).
32. Yehya, N. et al. Identification of molecular subphenotypes in two cohorts of paediatric ARDS. *Thorax* **79**, 128–134. https://doi.org/10.1136/thorax-2023-220130 (2024).
33. Shi, J. G. et al. The pharmacokinetics, pharmacodynamics, and safety of baricitinib, an oral JAK 1/2 inhibitor, in healthy volunteers. *J. Clin. Pharmacol.* **54**, 1354–1361. https://doi.org/10.1002/jcph.354 (2014).
34. Hoisnard, L. et al. Adverse events associated with JAK inhibitors in 126,815 reports from the WHO pharmacovigilance database. *Sci. Rep.* **12**, 7140. https://doi.org/10.1038/s41598-022-10777-w (2022).
35. Talasila, S., Lee, E., Teichner, E. M., Siegfried, E. C. & Jackson Cullison, S. R. Analysis of publicly available adverse events reported for pediatric patients treated with Janus kinase inhibitors. *Pediatr. Dermatol.* **41**, 1040–1046. https://doi.org/10.1111/pde.15721 (2024).
36. Gerard, L. et al. Airway epithelium damage in acute respiratory distress syndrome. *Crit. Care* **28**, 350. https://doi.org/10.1186/s13054-024-05127-3 (2024).
37. Yonis, H., Mortaza, S., Baboi, L., Mercat, A. & Guerin, C. Expiratory flow limitation assessment in patients with acute respiratory distress syndrome. A reappraisal. *Am. J. Respir. Crit. Care Med.* **198**, 131–134. https://doi.org/10.1164/rccm.201711-2326LE (2018).
38. Guerin, C., Cour, M. & Argaud, L. Airway closure and expiratory flow limitation in acute respiratory distress syndrome. *Front Physiol.* **12**, 815601. https://doi.org/10.3389/fphys.2021.815601 (2021).
39. Carlier, F. M., de Fays, C. & Pilette, C. Epithelial barrier dysfunction in chronic respiratory diseases. *Front Physiol.* **12**, 691227. https://doi.org/10.3389/fphys.2021.691227 (2021).
40. Dalton, C. M., Schlegel, C. & Hunter, C. J. Caveolin-1: A review of intracellular functions, tissue-specific roles, and epithelial tight junction regulation. *Biology (Basel)* https://doi.org/10.3390/biology12111402 (2023).
41. Qu, L. et al. Caveolin-1 identified as a key mediator of acute lung injury using bioinformatics and functional research. *Cell Death Dis.* **13**, 686. https://doi.org/10.1038/s41419-022-05134-8 (2022).
42. Xu, S., Xue, X., You, K. & Fu, J. Caveolin-1 regulates the expression of tight junction proteins during hyperoxia-induced pulmonary epithelial barrier breakdown. *Respir Res.* **17**, 50. https://doi.org/10.1186/s12931-016-0364-1 (2016).
43. Garrean, S. et al. Caveolin-1 regulates NF-kappaB activation and lung inflammatory response to sepsis induced by lipopolysaccharide. *J. Immunol.* **177**, 4853–4860. https://doi.org/10.4049/jimmunol.177.7.4853 (2006).
44. Jin, Y. et al. Caveolin-1 regulates the secretion and cytoprotection of Cyr61 in hyperoxic cell death. *FASEB J.* **23**, 341–350. https://doi.org/10.1096/fj.08-108423 (2009).
45. Jin, Y. et al. Deletion of caveolin-1 protects against oxidative lung injury via up-regulation of heme oxygenase-1. *Am. J. Respir. Cell Mol. Biol.* **39**, 171–179. https://doi.org/10.1165/rcmb.2007-0323OC (2008).
46. Jin, Y., Lee, S. J., Minshall, R. D. & Choi, A. M. Caveolin-1: A critical regulator of lung injury. *Am. J. Physiol. Lung Cell Mol. Physiol.* **300**, L151-160. https://doi.org/10.1152/ajplung.00170.2010 (2011).
47. Zhang, M. et al. Caveolin-1 mediates Fas-BID signaling in hyperoxia-induced apoptosis. *Free Radic. Biol. Med.* **50**, 1252–1262. https://doi.org/10.1016/j.freeradbiomed.2011.02.031 (2011).
48. Lee, J. W. et al. Acute lung injury edema fluid decreases net fluid transport across human alveolar epithelial type II cells. *J. Biol. Chem.* **282**, 24109–24119. https://doi.org/10.1074/jbc.M700821200 (2007).
49. Olman, M. A. et al. Pulmonary edema fluid from patients with early lung injury stimulates fibroblast proliferation through IL-1 beta-induced IL-6 expression. *J. Immunol.* **172**, 2668–2677. https://doi.org/10.4049/jimmunol.172.4.2668 (2004).
50. Pugin, J., Verghese, G., Widmer, M. C. & Matthay, M. A. The alveolar space is the site of intense inflammatory and profibrotic reactions in the early phase of acute respiratory distress syndrome. *Crit. Care Med.* **27**, 304–312. https://doi.org/10.1097/00003246-199902000-00036 (1999).
51. Ware, L. B. & Matthay, M. A. The acute respiratory distress syndrome. *N. Engl. J. Med.* **342**, 1334–1349. https://doi.org/10.1056/NEJM200005043421806 (2000).
52. Pittet, J. F. et al. Reactive nitrogen species inhibit alveolar epithelial fluid transport after hemorrhagic shock in rats. *J. Immunol.* **166**, 6301–6310. https://doi.org/10.4049/jimmunol.166.10.6301 (2001).
53. Williams, A. E. et al. Evidence for chemokine synergy during neutrophil migration in ARDS. *Thorax* **72**, 66–73. https://doi.org/10.1136/thoraxjnl-2016-208597 (2017).
54. Standiford, T. J. et al. Macrophage inflammatory protein-1 alpha mediates lung leukocyte recruitment, lung capillary leak, and early mortality in murine endotoxemia. *J. Immunol.* **155**, 1515–1524 (1995).
55. Bhatia, M., Zemans, R. L. & Jeyaseelan, S. Role of chemokines in the pathogenesis of acute lung injury. *Am. J. Respir. Cell Mol. Biol.* **46**, 566–572. https://doi.org/10.1165/rcmb.2011-0392TR (2012).
56. Ichikawa, A. et al. CXCL10-CXCR3 enhances the development of neutrophil-mediated fulminant lung injury of viral and nonviral origin. *Am. J. Respir. Crit. Care Med.* **187**, 65–77. https://doi.org/10.1164/rccm.201203-0508OC (2013).
57. Lang, S. et al. CXCL10/IP-10 neutralization can ameliorate lipopolysaccharide-induced acute respiratory distress syndrome in rats. *PLoS ONE* **12**, e0169100. https://doi.org/10.1371/journal.pone.0169100 (2017).
58. Wang, W. et al. Monoclonal antibody against CXCL-10/IP-10 ameliorates influenza A (H1N1) virus induced acute lung injury. *Cell Res.* **23**, 577–580. https://doi.org/10.1038/cr.2013.25 (2013).
59. Hue, S. et al. Uncontrolled innate and impaired adaptive immune responses in patients with COVID-19 acute respiratory distress syndrome. *Am. J. Respir. Crit. Care Med.* **202**, 1509–1519. https://doi.org/10.1164/rccm.202005-1885OC (2020).
60. Uchida, T. et al. Receptor for advanced glycation end-products is a marker of type I cell injury in acute lung injury. *Am. J. Respir. Crit. Care Med.* **173**, 1008–1015. https://doi.org/10.1164/rccm.200509-1477OC (2006).
61. Briot, R. et al. Elevated levels of the receptor for advanced glycation end products, a marker of alveolar epithelial type I cell injury, predict impaired alveolar fluid clearance in isolated perfused human lungs. *Chest* **135**, 269–275. https://doi.org/10.1378/chest.08-0919 (2009).
62. Calfee, C. S. et al. Plasma receptor for advanced glycation end products and clinical outcomes in acute lung injury. *Thorax* **63**, 1083–1089. https://doi.org/10.1136/thx.2008.095588 (2008).
63. Jabaudon, M. et al. Soluble receptor for advanced glycation end-products predicts impaired alveolar fluid clearance in acute respiratory distress syndrome. *Am. J. Respir. Crit. Care Med.* **192**, 191–199. https://doi.org/10.1164/rccm.201501-0020OC (2015).
64. Jain, N. K. et al. Therapeutic implications of current Janus kinase inhibitors as anti-COVID agents: A review. *Front Pharmacol.* **14**, 1135145. https://doi.org/10.3389/fphar.2023.1135145 (2023).

65. Wolfe, C. R. et al. Baricitinib versus dexamethasone for adults hospitalised with COVID-19 (ACTT-4): A randomised, double-blind, double placebo-controlled trial. *Lancet Respir. Med.* **10**, 888–899. https://doi.org/10.1016/S2213-2600(22)00088-1 (2022).
66. Bronte, V. et al. Baricitinib restrains the immune dysregulation in patients with severe COVID-19. *J. Clin. Invest.* **130**, 6409–6416. https://doi.org/10.1172/JCI141772 (2020).
67. Davis, J. D. & Wypych, T. P. Cellular and functional heterogeneity of the airway epithelium. *Mucosal. Immunol.* **14**, 978–990. https://doi.org/10.1038/s41385-020-00370-7 (2021).
68. Tata, P. R. et al. Dedifferentiation of committed epithelial cells into stem cells in vivo. *Nature* **503**, 218–223. https://doi.org/10.1038/nature12777 (2013).
69. Basil, M. C. et al. The cellular and physiological basis for lung repair and regeneration: Past, present, and future. *Cell Stem Cell* **26**, 482–502. https://doi.org/10.1016/j.stem.2020.03.009 (2020).
70. Celli, B. R. & Owen, C. A. The club cell and its protein, CC16: Time to shine. *Lancet Respir. Med.* **1**, 757–759. https://doi.org/10.1016/S2213-2600(13)70247-9 (2013).
71. Broeckaert, F. & Bernard, A. Clara cell secretory protein (CC16): Characteristics and perspectives as lung peripheral biomarker. *Clin. Exp. Allergy* **30**, 469–475. https://doi.org/10.1046/j.1365-2222.2000.00760.x (2000).
72. Janicova, A. et al. Endogenous uteroglobin as intrinsic anti-inflammatory signal modulates monocyte and macrophage subsets distribution upon sepsis induced lung injury. *Front Immunol.* **10**, 2276. https://doi.org/10.3389/fimmu.2019.02276 (2019).
73. Recchia Luciani, G. et al. IRF1 mediates growth arrest and the induction of a secretory phenotype in alveolar epithelial cells in response to inflammatory cytokines IFNgamma/TNFalpha. *Int. J. Mol. Sci.* https://doi.org/10.3390/ijms25063463 (2024).
74. Emeriaud, G. et al. Executive summary of the second international guidelines for the diagnosis and management of pediatric acute respiratory distress syndrome (PALICC-2). *Pediatr. Crit. Care Med.* **24**, 143–168. https://doi.org/10.1097/PCC.0000000000003147 (2023).
75. Leteurtre, S. et al. PELOD-2: An update of the PEdiatric logistic organ dysfunction score. *Crit. Care Med.* **41**, 1761–1773. https://doi.org/10.1097/CCM.0b013e31828a2bbd (2013).
76. Pollack, M. M., Patel, K. M. & Ruttimann, U. E. PRISM III: An updated pediatric risk of mortality score. *Crit. Care Med.* **24**, 743–752. https://doi.org/10.1097/00003246-199605000-00004 (1996).

Acknowledgements

Research reported in this publication was supported in part by the Emory University Integrated Cellular Imaging Core and Children's Healthcare of Atlanta, (RRID:SCR_023534). The content is solely the responsibility of the authors and does not necessarily reflect the official views of the National Institute of Health. Children's Healthcare of Atlanta and Emory University's the Children's Healthcare of Atlanta Center for Clinical and Translational (CCTR) provided financial support with a pilot award (Project Number 00130746) to JG. We are grateful to Dr. Shuichi Takayama, PhD for his discussions regarding the model experiments and review of the final manuscript.

Author contributions

JG and AF conceived and developed the study, supervised the acquisition of the biological data, analyzed and interpreted the data. JG and AF drafted and edited the manuscript. SS developed model methodology. SS and GD helped with patient sample processing, performed experiments and edited the manuscript. BD helped with model development and experiments. CZ and NJ assisted in identifying, consenting, acquiring patient samples and assisted in collecting clinical information about the patients. All authors edited and approved the final version of this manuscript.

Funding

Funding was provided by NIH grants K23 HL151897 and R01 HL171627 to JG. Emory University's the Children's Healthcare of Atlanta Center for Clinical and Translational (CCTR) provided financial support with a pilot award (Project Number 00130746) to JG. Funding was provided by the NIH grant K24 NR018866 and R01 NR018666 to AF. BD was supported by an NIH grant T32 GM145735.

Declarations

Competing interests

The authors declare no competing interests.

Institutions where work was performed

Emory University School of Medicine, Children's Healthcare of Atlanta.

Additional information

Correspondence and requests for materials should be addressed to J.R.G.